Journal of Power Sources 195 (2010) 3105–3110

Contents lists available at ScienceDirect

Journal of Power Sources

journal homepage: www.elsevier.com/locate/jpowsour

Pt nanoparticles deposited on TiO_2 based nanofibers: Electrochemical stability and oxygen reduction activity

Alex Bauer, Kunchan Lee, Chaojie Song, Yongsong Xie, Jiujun Zhang, Rob Hui*

Institute for Fuel Cell Innovation, National Research Council of Canada, 4250 Wesbrook Mall, Vancouver, B.C., Canada V6T 1W5

ARTICLE INFO

Article history:
Received 14 October 2009
Received in revised form
23 November 2009
Accepted 25 November 2009
Available online 1 December 2009

Keywords:
Ceramic catalyst supports
Nanofibers
Electrochemical stability
Platinum
Oxygen reduction reaction

ABSTRACT

The electrochemical stability of Pt deposited on TiO_2 based nanofibers was compared with commercially available carbon supported Pt. Prior to the Pt deposition the TiO_2 material, which was either undoped or Nb doped, was air calcined. In one case the undoped TiO_2 was also reduced in a hydrogen atmosphere. XRD analysis revealed that the unreduced TiO_2 was present in the anatase phase, irrespective of whether the Nb dopant was present, whereas the rutile phase was formed due to reduction with H_2. The diameter of the TiO_2 fibers varied from 50 to 100 nm, and the average Pt particle diameter was approximately 5 nm. Pt supported on TiO_2 was more stable than Pt supported on C when subjected to 1000 voltammetric cycles in the range of 0.05–1.3 V vs. RHE. Nb doped TiO_2 showed the highest stability, retaining 60% of the electrochemically active surface area after 1000 cycles compared to the state after 100 cycles, whereas the carbon supported catalyst retained 20% of the active surface area. The commercial catalyst had the highest oxygen reduction activity due to its larger specific area (17.1 $m^2\,g^{-1}$ vs. 5.0 $m^2\,g^{-1}$ for Pt/TiO_2–Nb, measured after 100 cycles) and the higher support conductivity. The Pt supported on Nb doped or on H_2 reduced TiO_2 was more active than Pt supported on air calcined and otherwise unmodified TiO_2.

Crown Copyright © 2009 Published by Elsevier B.V. All rights reserved.

1. Introduction

There are several advantages to operating hydrogen PEM fuel cells at temperatures above 100 °C. The rate of the electrochemical conversion of the oxidant and fuel to water is increased, heat and water management are simplified, and there is a higher tolerance for fuel impurities (e.g., CO from natural gas reforming). Conventional Nafion® membranes are not applicable for these high temperature conditions due to drying, inherent loss of conductivity and degradation. Therefore the development of membrane materials, which meet the operation requirements in terms of conductivity and durability, is necessary [1–3]. Another severe problem that compromises the fuel cell durability is carbon corrosion, which occurs at potentials higher than 0.9 V vs. RHE according to Eq. (1) [4]:

$$C + 2H_2O \rightarrow CO_2 + 4H^+ + 4e^- \quad (1)$$

This degradation process is more pronounced at elevated temperatures, and it is particularly detrimental in the case of automotive fuel cell applications where the cell voltage can reach 1.5 V during start-up-shutdown cycles [5]. A significant loss of the active catalyst area occurs when the carbon support disintegrates [6]. Therefore it is important to identify alternative support materials that are cost effective while providing sufficient electronic conductivity and electrochemical stability. Alternative support materials (i.e., conductive ceramics, such as titanium, tungsten and zirconium oxides) with dimensions in the nanometer range were proposed in the literature [7]. For example, TiO_2 nanoparticles were synthesized by a sol–gel method and then platinized [8]. The TiO_2 supported catalyst showed similar performance compared to carbon supported Pt in a H_2 PEM fuel cell when operated at 60 °C and 0.8 V. However, in the Ohmic regime the application of the ceramic support yielded lower performance due to its higher electrical resistance. Forno et al. employed a reflux method to grow either Pt nanoparticles or nanowires on titania nanofibers [9]. The Pt nanowires had an approximate diameter of 7 nm and lengths of up to 125 nm. The surface coverage with Pt nanoparticles, which had a diameter of 2 nm, could be increased by extending the deposition time. Several studies focused on utilizing TiO_2 supported Pt for the relatively sluggish oxygen reduction reaction (ORR), one of the main limiting factors with respect to the PEM fuel cell performance [4,10,11]. Lee et al. described the fabrication of TiO_2 nanotubes onto which Pt was deposited through either sputtering or evaporation. The sputtered catalyst outperformed the Pt obtained by evaporation as indicated by a ~0.05 V shift of the ORR onset potential.

Abbreviations: ORR, oxygen reduction reaction; PEM, proton exchange membrane; RDE, rotating disk electrode; RHE, reversible hydrogen electrode; TEM, transmission electron microscopy; XRD, X-ray diffraction.

* Corresponding author. Tel.: +1 604 221 3111; fax: +1 604 221 3001.
E-mail address: rob.hui@nrc-cnrc.gc.ca (R. Hui).

0378-7753/$ – see front matter. Crown Copyright © 2009 Published by Elsevier B.V. All rights reserved.
doi:10.1016/j.jpowsour.2009.11.107

Nomenclature

E	electrode potential [V vs. RHE]
i	current density per geometric electrode area [A cm^{-2}]

Huang et al. reported very promising fuel cell polarization data. They showed that Pt dispersed on mesoporous TiO_2 yielded similar performance as a carbon supported Pt catalyst [12]. At current densities below 1 A cm^{-2} the Pt/C catalyst yielded a slightly higher cell voltage. However, the peak power density was increased by ~12% with the TiO_2 supported catalyst. Under potentiostatic fuel cell operation at 1.2 V, a loss of 100 mV was observed for the conventional catalyst after 50 h, whereas the titania supported Pt was fully stable for 200 h.

TiO_2 may also improve the Pt oxygen reduction activity through facilitating mechanisms, such as reactant surface diffusion and oxygen spill-over [13].

The TiO_2 support conductivity can be improved by reduction in a hydrogen atmosphere at elevated temperature (e.g., 500–600 °C) whereby substoichiometric titanium oxide (TiO_{2-x}) is formed. Thus, a certain fraction of Ti^{3+} species is present in the TiO_2 lattice [14]. Another approach to improving the conductivity is the introduction of dopants, such as Nb or Ta, which have a higher valence state than Ti^{4+} [4,15]. Doping of TiO_2 is also beneficial for other applications such as gas sensors [16] or dye-sensitized solar cells [17].

The main objective of this work is to characterize the electrochemical stability and oxygen reduction activity of TiO_2 nanofiber supported Pt catalysts relative to conventional carbon supported Pt. Furthermore, the effects of support modification by either H_2 treatment or Nb doping on the electrochemical stability and oxygen reduction performance were investigated. This work is a preliminary study, as the target application for such catalyzed fibers is PEM fuel cell operation at temperatures in excess of 100 °C. The fibrous TiO_2 was produced by a simple electrospinning process [18–20]. Electrospinning of nanofibers can be utilized for a variety of applications, e.g., filtration, tissue engineering scaffolds, wound healing, drug release control, and energy storage [21,22]. Catalyzed TiO_2 nanofibers were also proposed for utilization in heterogeneous catalysis, e.g., for the water gas shift reaction [23].

2. Experimental

2.1. Fabrication of TiO_2 nanofibers

Electrospinning of the TiO_2 nanofibers was carried out in air at 20 °C with a standard syringe and grounded collector plate configuration, as described in the literature [18,21]. To prepare the precursor solution, 0.3 g polyvinyl pyrrolidone (Alfa Aesar) was added to 7.5 ml of anhydrous ethanol (Commercial Alcohols Inc.) and stirred until it was completely dissolved. A second solution was prepared by mixing 1.5 g of titanium(IV)isopropoxide (98%, Acros), 3 ml of acetic acid (Fisher) and 3 ml of anhydrous ethanol. To prepare the Nb doped TiO_2, 0.18 g of niobium ethoxide (99.99%, Alfa Aesar) was also added (approximately 10 mol% of the total number of Nb and Ti atoms). The solutions were degassed by sonicating for 20 min and then mixed together and poured into the syringe. This precursor solution was fed at a constant feed rate of 0.7 ml h^{-1} through a stainless steel needle with a flat outlet. The distance between the tip of the needle and the collector plate was 6 cm, and the applied voltage was 11.55 kV. Due to the external electrostatic field and the electrostatic repulsion between the surface charges, a so-called Taylor cone is formed at the tip of the needle instead of a droplet [18]. During electrospinning the effects of the surface tension are outbalanced by the electrostatic interactions and a liquid jet is formed, which is transformed into a thin elongated thread that is directed towards the collector plate. The needle was slowly moved along two perpendicular paths to randomly deposit the TiO_2 fibers on a stainless steel mesh, which was placed on top of the aluminum collector plate. Over time a white mat of fibers was obtained. The electrospun fibers were exposed to air at 20 °C for several hours to allow for the complete hydrolysis of the polymer. In each case this step was followed by calcination in air at 500 °C for 3 h to completely decompose and remove the precursor residues. The undoped TiO_2 fibers were either used as Pt substrates without further modification or reduced in a hydrogen gas stream at 650 °C for 3 h.

2.2. Pt nanoparticle deposition

50 mg of H_2PtCl_6 (Sigma–Aldrich) and 90 mg TiO_2 nanofibers were combined with 75 ml of ethylene glycol. The pH-value was adjusted to 10 by drop-wise addition of NaOH (1 M in ethylene glycol). To reduce the Pt salt, 16 ml of 0.1 M $NaBH_4$ in ethylene glycol was added, followed by stirring for 2 h at 20 °C [24]. The Pt coated fibers were separated from the ethylene glycol solvent with a centrifuge (operated at 11,000 rpm for 9 min). The ethylene glycol was removed and replaced with deionized water and centrifugation was repeated. To completely remove the ethylene glycol this step was repeated three more times. The fibers were dried in an oven at 80 °C overnight. The Pt catalyst was then reduced in a furnace under a hydrogen stream (50 vol% in N_2) at 300 °C for 3 h.

2.3. X-ray analysis

XRD measurements were carried out with uncatalyzed TiO_2 nanofibers using a Bruker D8 diffractometer with Cu-Kα radiation. The fibers were pressed onto a glass plate to form compact powders.

2.4. Imaging

Transmission electron microscopy was conducted with a Hitachi H7600 microscope, operated at 100 kV, at the BioImaging facilities located in the Biology Department of the University of British Columbia.

2.5. Electrochemical testing

All electrochemical experiments were performed with a Solartron multistat instrument (controlled with Corrware software, Scribner Associates Inc., USA) and a three-electrode set-up contained in a glass cell. All electrochemical experiments were carried out at 20 °C and ambient pressure. The working electrode was a glassy carbon rotating disk electrode (RDE) (Pine Instrument), and a $Hg/HgSO_4$ reference electrode containing 30 wt% sulfuric acid (Koslow Scientific) was used. A Pt wire functioned as the counter electrode. The catalyst powder was dispersed in deionized water by sonication for 20 min before depositing the selected loading of 62 μg cm^{-2} (corresponding to a Pt loading of 12 μg cm^{-2} or 20 wt%) onto the electrode with a micropipette. A Nafion film was cast by pipetting 5 μl of a 0.07 wt% Nafion solution onto the powder coated RDE. To clean the Pt surface each freshly prepared electrode was cycled 20 times in a N_2 purged 0.5 M H_2SO_4 electrolyte in the range of 0.05–1.2 V vs. RHE at a scan rate of 50 mV s^{-1}. To study the catalyst stability, cyclic voltammetry was carried out at 100 mV s^{-1}, performing 1000 full cycles in the range of 0.05–1.3 V vs. RHE. After 100, 500 and 1000 cycles the active surface Pt area was estimated based on the H_2 desorption peaks observed between 0.05 and 0.35 V vs. RHE. A hydrogen desorption charge of 210 μC cm^{-2}

was assumed for the active Pt area calculation [25]. Monitoring Pt surface area decrease during extended cycling allowed for assessing the catalyst stability.

Voltammetric oxygen reduction experiments were carried out with an O_2 saturated 0.5 M H_2SO_4 electrolyte at a scan rate of 5 mV s^{-1}. The rotation rate was 400 rpm. The potential was decreased from 1.0 V vs. RHE to 0.05 V vs. RHE and then ramped back to the initial potential. In this paper the current density is reported as current per geometric electrode area.

3. Results and discussion

3.1. XRD analysis

XRD measurements were performed on air calcined fibers, which were either undoped or doped with Nb, to determine whether the Nb dopant was fully incorporated into the TiO_2 lattice. Fig. 1a and b shows the presence of the anatase phase. No additional peaks were observed for the Nb doped sample compared to undoped TiO_2. Therefore it can be assumed that the Nb atoms fully were incorporated into the TiO_2 lattice. It was reported that the transition from the anatase to the rutile phase in air does not occur at temperatures below 700 °C [20,26]. XRD measurements carried out by Ruiz et al. indicated that in the case of the anatase phase a mole fraction of at least 10% Nb could be incorporated into the TiO_2 lattice, while for rutile the Nb solubility limit was 6% [27]. Furthermore, the rutile structure was formed by the hydrogen reduction treatment of the undoped TiO_2 sample, as shown in Fig. 1c.

3.2. TEM imaging

The TEM micrographs in Fig. 2 show TiO_2 nanofibers with Pt nanoparticles dispersed on the surface. The fiber diameter varied from 50 to 100 nm, as indicated in Fig. 2a. The approximate average Pt nanoparticle diameter was 5 nm. In the case of the H_2 reduced sample (Fig. 2b) the dispersion of the Pt nanoparticles was less homogeneous compared with the other samples. This observation can be rationalized by the lower surface roughness (i.e., a lower amount of nucleation sites on the surface) of the H_2 reduced substrate. A certain degree of agglomeration was observed in each case with a more pronounced agglomeration found for the undoped samples (compare Fig. 2b and c, for example).

3.3. Electrochemical measurements

The voltammograms presented in Fig. 3 show that the active Pt area decreased as a consequence of continuous cycling. This trend is indicated, for example, by the hydrogen desorption peaks present in the potential range of 0.05–0.35 V vs. RHE. The voltammograms obtained with titania supported Pt show a distinct double layer region with a quasi-constant current in the range of 0.35–0.65 V vs. RHE (anodic scans in Fig. 3b and c). By contrast, the voltammetric measurements performed with the carbon supported catalyst yielded a peak at 0.65 V vs. RHE for the anodic sweep (Fig. 3a). This peak likely represents an interaction with acidic functional groups on the carbon surface. Furthermore, for the cathodic sweep a convoluted peak was observed at 0.75 V for the 100th and 500th cycle, respectively. After 1000 cycles the peak at 0.75 V was reduced to a shoulder, and a subtle peak remained at 0.62 V. It is hypothesized that these cathodic features at 0.75 and 0.62 V represent the reduction of platinum oxide and interactions with functional groups on the carbon surface, respectively. The decline of the platinum oxide reduction peak implies a significant loss of Pt active sites over 1000 cycles. This hypothesis is corroborated by the decrease of the hydrogen desorption current, e.g., at an electrode potential of 0.12 V.

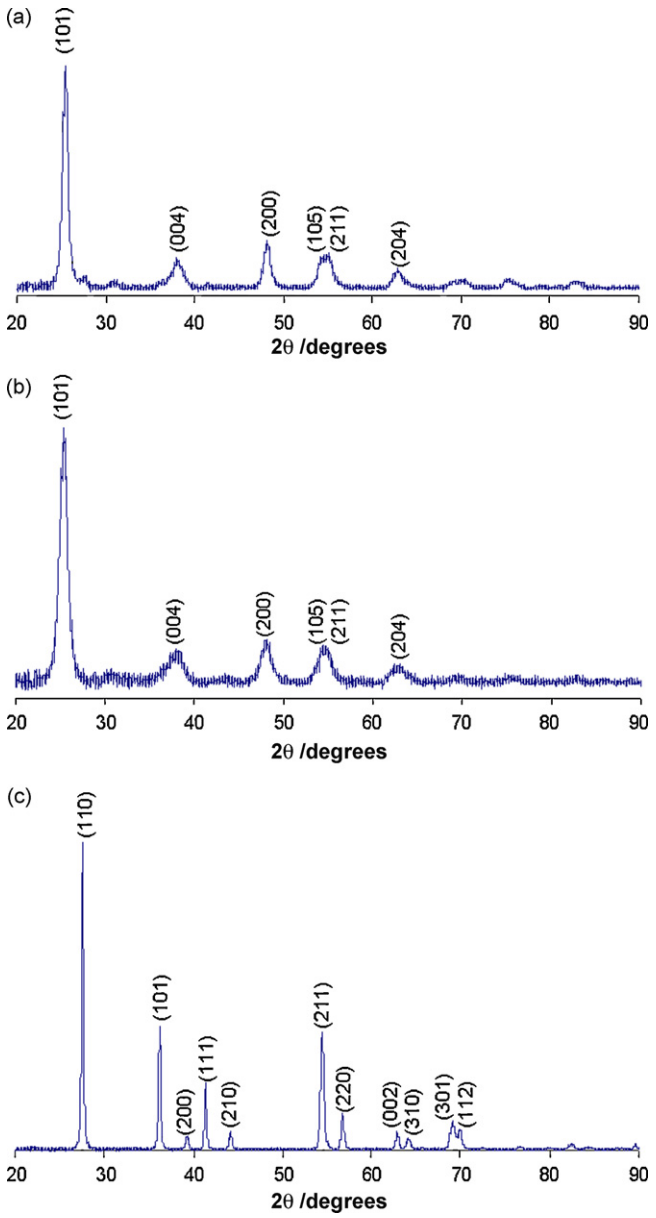

Fig. 1. XRD spectra for undoped (a) and Nb doped (b) TiO_2 nanofibers (both samples were calcined in air at 500 °C), as well as for undoped TiO_2 nanofibers reduced in H_2 at 650 °C (c).

The hydrogen desorption regime was evaluated for the active Pt area estimation as described in Section 2.5. The commercially available carbon supported Pt catalyst (E-tek) was compared with the different TiO_2 supported Pt samples in terms of stability by assessing the active Pt area after 100, 500 and 1000 cycles (Fig. 4). The active Pt area of the commercial catalyst measured after the first 100 cycles (17.1 m^2 g^{-1}) was significantly higher than that of the TiO_2 supported catalysts (1.3–5.0 m^2 g^{-1}). After 1000 cycles the active Pt surface area for Pt/C (3.4 m^2 g^{-1}) was comparable to that of Pt/TiO_2–Nb (3.0 m^2 g^{-1}).

The state of the electrode after 100 cycles was arbitrarily selected as a base case for a comparison of the relative loss of the active Pt surface due to extended cycling. Fig. 5 shows that the carbon supported catalyst deteriorated more severely compared with the cases in which TiO_2 was applied, as only 20% of the active Pt surface area remained after 1000 cycles compared to the state after 100 cycles. Among the titania supported catalysts the Nb doped sample had the highest stability, since 60% of the active Pt area

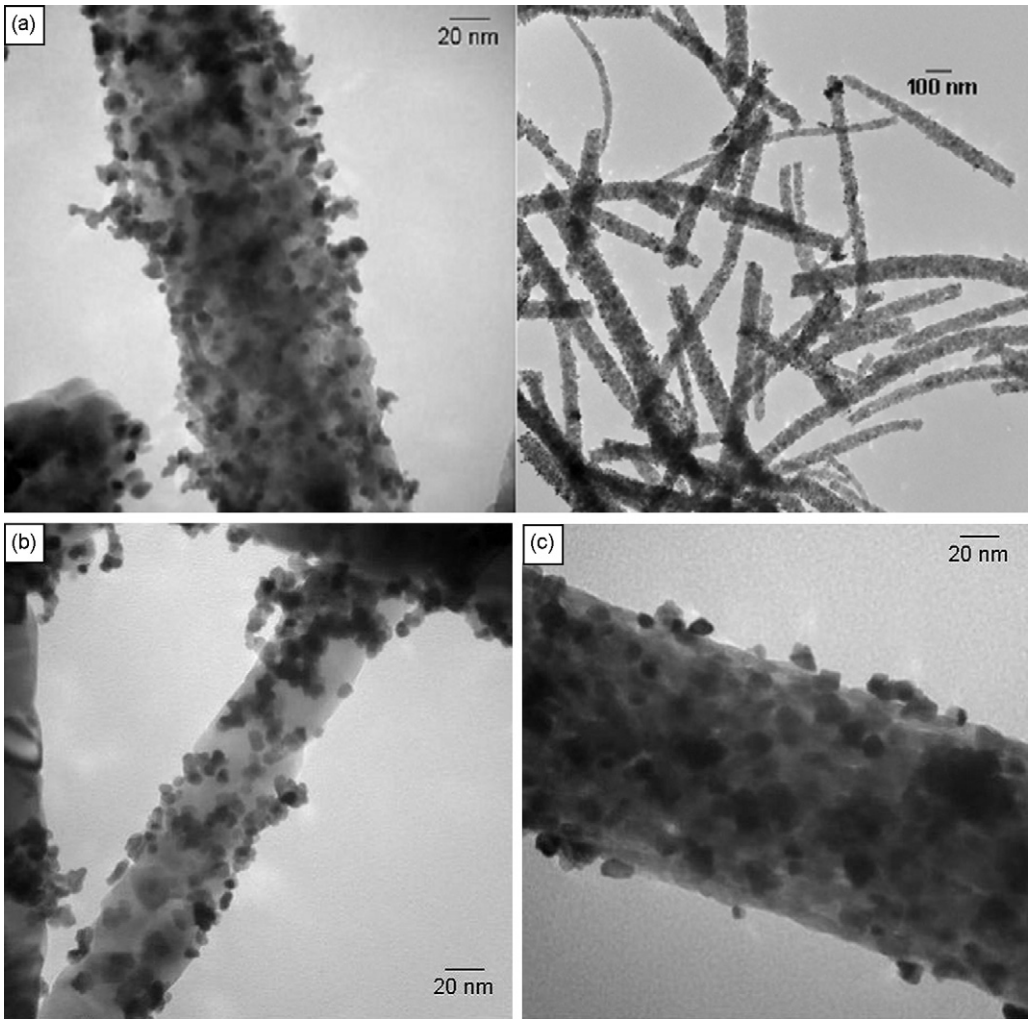

Fig. 2. TEM micrographs of Pt nanoparticles deposited onto TiO_2 nanofibers. Before the Pt deposition the fibers had been treated by calcination in air at 500 °C (a), reduction in H_2 at 650 °C (after calcination in air) (b), and Nb doping (10 mol%) (also calcined in air) (c).

was still available after 1000 cycles. On the other hand the air calcined undoped TiO_2 was the least stable sample with 32% of the active area remaining after 1000 cycles. All TiO_2 based samples can be considered more electrochemically stable than the commercial catalyst under the employed experimental conditions. The relatively high degree of stability of the Nb doped support may be attributed to the differences of the electronic conductivities associated with the different materials. Both Nb doped and reduced TiO_2 have higher electronic conductivity than the air calcined TiO_2 due to the presence of Ti^{3+} species [14,27,28]. The TiO_2 material reduced in H_2 has the highest conductivity among the ceramic materials tested in this work. The Ti^{3+} in reduced TiO_2 was produced by reduction of Ti^{4+} and therefore left an oxygen deficient metastable structure. The Ti^{3+} produced by Nb doping was stabilized as a consequence of the electronic neutrality requirement when Ti^{4+} was partially replaced with Nb^{5+}. Therefore the Ti^{3+} produced with H_2 reduction may be less stable than the Ti^{3+} produced through doping. In the presence of the mixed valance states of Ti^{3+} and Ti^{4+}, a strong metal-support interaction has been reported for Pt/TiO_2 compounds [29–31]. Although a strong metal-support interaction might be present in the case of the TiO_2 nanofibers, it has not been observed with the experimental methods applied in this work.

Chhina et al. performed potentiostatic stability tests with a fuel cell operated at 85 °C and 1.4 V for 20 h [10]. Pt (10 wt%) on Nb doped TiO_2 was compared with a commercially available Pt catalyst (40 wt% on Vulcan XC-72R carbon). The initial and final states of the respective catalysts were characterized by in situ cyclic voltammetry in the range of 0.05–1.4 V relative to the anode, which functioned as a quasi reference electrode. The degradation of the ceramic supported catalyst was minimal, whereas the carbon degradation was significant, as indicated by the respective hydrogen desorption peaks.

The oxygen reduction experiments presented in Fig. 6 show that the commercial carbon supported catalyst yielded the best performance due to its higher specific Pt surface area (see also Fig. 4) and the relatively high conductivity of the carbon support. By contrast, experimental data reported by Park and Seol [4] and Chhina et al. [10] showed an improvement in the oxygen reduction activity with Nb doped TiO_2 supports compared to Pt/C. In our work we observed an improvement of the activity due to either Nb doping or H_2 reduction compared to the unmodified air calcined Pt/TiO_2. This behavior was likely due to the improved electronic conductivity of the catalyst support [4].

XPS data reported by Ruiz et al. showed that the valence band edge of TiO_2 is shifted to higher binding energies in the presence of Nb [27]. This implies an increase in conductivity, as the Fermi level is shifted closer to the conduction band. Another important observation is that the specific Pt surface areas of the doped and H_2 reduced TiO_2 supported catalysts were significantly larger than that of the air calcined sample.

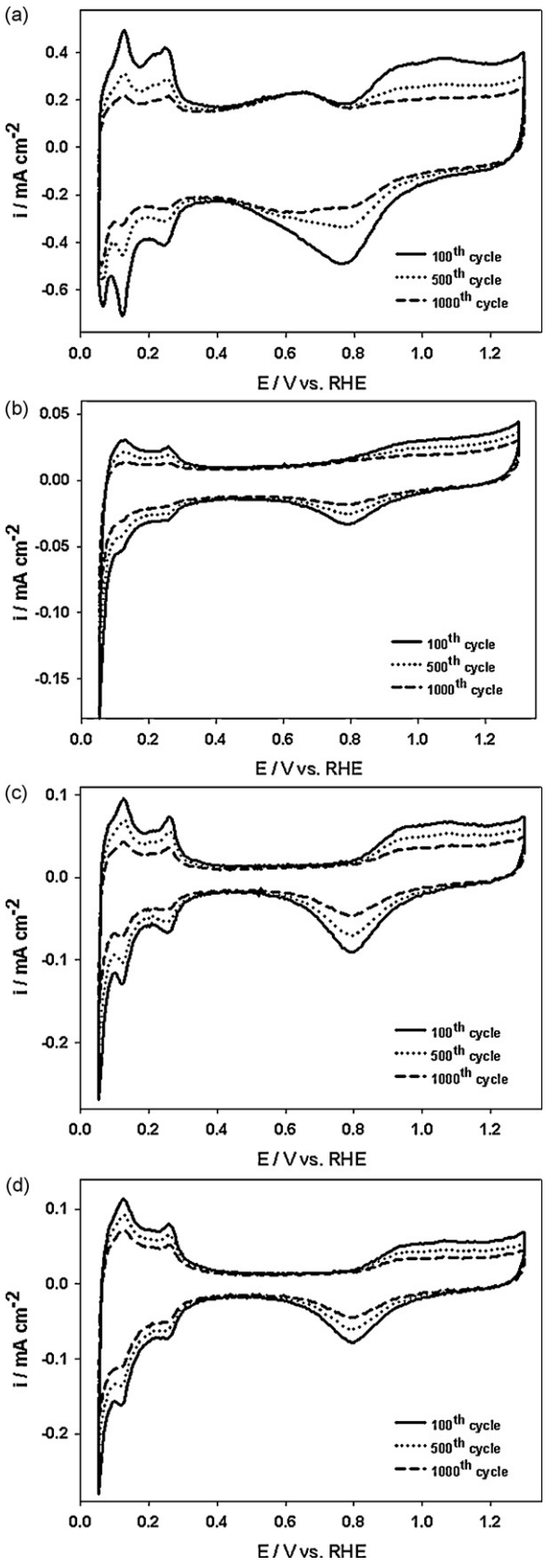

Fig. 3. Cyclic voltammograms obtained after 100, 500 and 1000 cycles for commercial Pt/C (E-tek) (a), Pt/air calcined TiO_2 (b), Pt/H_2 reduced TiO_2 (c), Pt/Nb doped TiO_2 (d). Electrolyte: N_2 purged 0.5 M H_2SO_4, scan rate: 100 mV s^{-1}.

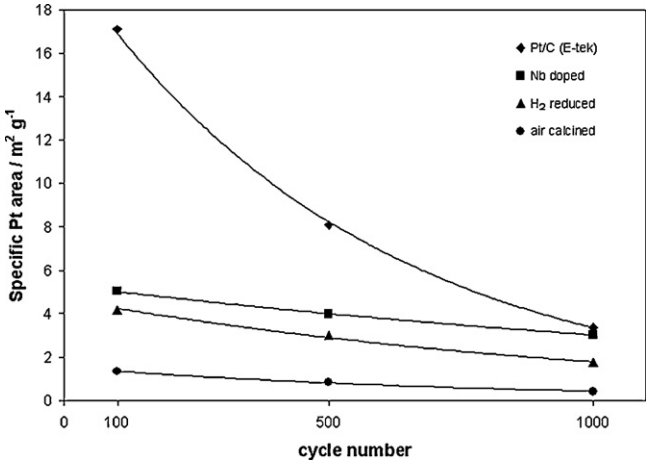

Fig. 4. Specific Pt surface area obtained from the hydrogen desorption peaks (see Fig. 3) as a function of the number of cycles in the range of 0.05–1.3 V vs. RHE.

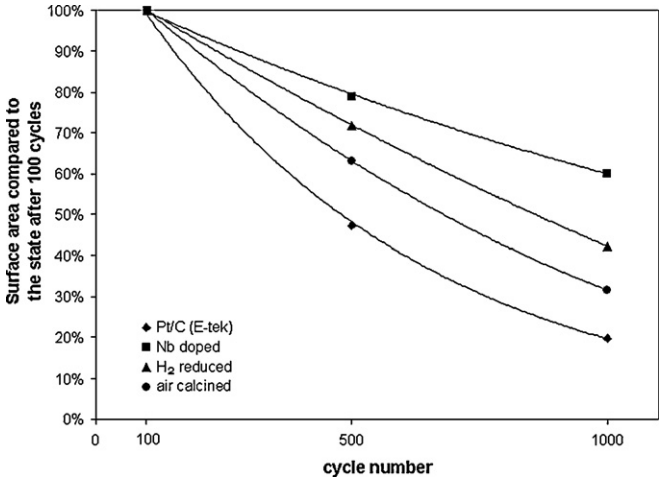

Fig. 5. Pt active surface area fraction remaining as a function of the number of voltammetric cycles. The state of the electrode after 100 cycles was defined as the initial state.

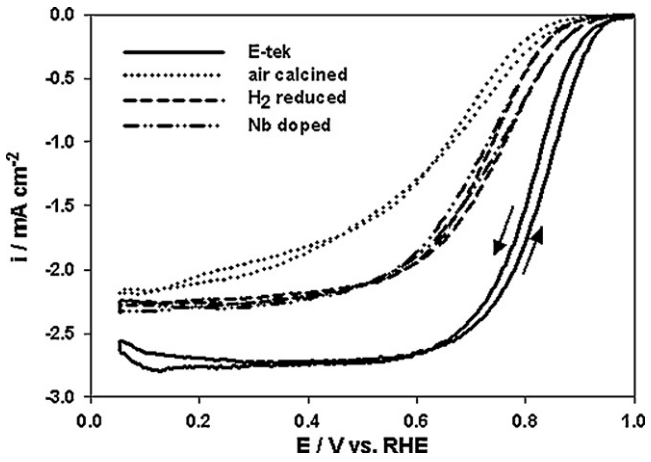

Fig. 6. Oxygen reduction experiments in oxygen saturated 0.5 M H_2SO_4. Scan rate: 5 mV s^{-1}, rotation rate: 400 rpm.

4. Conclusions

This work suggests that applying TiO_2 nanofibers as fuel cell catalyst supports can improve the catalyst durability compared to conventional carbon. The homogeneous dispersion of Pt nanoparticles onto the TiO_2 surface was achieved by reduction with $NaBH_4$ in an ethylene glycol based solution. Nb doping yielded the most promising results in terms of stability. After calcining in air the anatase phase was present in the case of the undoped and Nb doped support, as demonstrated by XRD. Hydrogen treatment of the undoped TiO_2 nanofibers at 650 °C yielded the rutile structure. The Nb doped and H_2 reduced TiO_2 supported catalysts outperformed the untreated TiO_2 based Pt in terms of ORR activity. The commercially available Pt/C catalyst had the highest activity due to the larger active surface area and the higher electronic conductivity of the support. Further tests are necessary to compare the activity of 'aged' carbon and metal oxide supported catalysts that were subjected to extended voltammetric cycling. Future work will also include fuel cell experiments at temperatures above 100 °C.

References

[1] J. Zhang, Z. Xie, J. Zhang, Y. Tang, C. Song, T. Navessin, Z. Shi, D. Song, H. Wang, D.P. Wilkinson, Z.-S. Liu, S. Holdcroft, J. Power Sources 160 (2006) 872–891.
[2] Q.F. Li, H.A. Hjuler, N.J. Bjerrum, J. Appl. Electrochem. 31 (2001) 773–779.
[3] J. Mosa, G. Larramona, A. Durán, M. Aparicio, J. Membr. Sci. 307 (2008) 21–27.
[4] K.-W. Park, K.-S. Seol, Electrochem. Commun. 9 (2007) 2256–2260.
[5] H. Chhina, D. Susac, S. Campbell, O. Kesler, Electrochem. Solid-State Lett. 12 (2009) B97–B100.
[6] X. Wang, W. Li, Z. Chen, M. Waje, Y. Yan, J. Power Sources 158 (2006) 154–159.
[7] E. Antolini, E.R. Gonzalez, Solid State Ionics 180 (2009) 746–763.
[8] N. Rajalakshmi, N. Lakshmi, K.S. Dhathathreyan, Int. J. Hydrogen Energy 33 (2008) 7521–7526.
[9] E. Forno, E. Lee, D. Campbell, Y. Xia, Nano Lett. 8 (2008) 668–672.
[10] H. Chhina, S. Campbell, O. Kesler, J. Electrochem. Soc. 156 (2009) B1232–B1237.
[11] W.-J. Lee, M. Alhosan, S.L. Yohe, N.L. Macy, W.H. Smyrl, J. Electrochem. Soc. 155 (2008) B915–B920.
[12] S.-Y. Huang, P. Ganesan, S. Park, B.N. Popov, J. Am. Chem. Soc. Commun. 131 (2009) 13898–13899.
[13] B. Hammer, J.K. Norskov, Adv. Catal. 45 (2000) 71–129.
[14] T. Berger, O. Diwald, E. Knözinger, F. Napoli, M. Chiesa, E. Giamello, Chem. Phys. 339 (2007) 138–145.
[15] U. Balachandran, N.G. Eror, J. Mater. Sci. 17 (1982) 1207–1212.
[16] R.K. Sharma, M.C. Bhatnagar, G.L. Sharma, Appl. Surf. Sci. 92 (1996) 647–650.
[17] S. Lee, J.H. Noh, H.S. Han, D.K. Yim, D.H. Kim, J.-K. Lee, J.Y. Kim, H.S. Jung, K.S. Hong, J. Phys. Chem. C 113 (2009) 6878–6882.
[18] D. Li, Y. Xia, Adv. Mater. 16 (2004) 1151–1170.
[19] D. Li, Y. Xia, Nano Lett. 3 (2003) 555–560.
[20] B. Ding, C.K. Kim, H.Y. Kim, M.K. Seo, S.J. Park, Fibers Polym. 5 (2004) 105–109.
[21] J. Fang, H.T. Niu, T. Lin, X.G. Wang, Chin. Sci. Bull. 53 (2008) 2265–2286.
[22] V. Beachley, X. Wen, Mater. Sci. Eng. C 29 (2009) 663–668.
[23] H. Kim, Y. Choi, N. Kanuka, H. Kinoshita, T. Nishiyama, T. Usami, Appl. Catal. A 352 (2009) 265–270.
[24] P. Kim, J.B. Joo, W. Kim, J. Kim, I.K. Song, J. Yi, J. Power Sources 160 (2006) 987–990.
[25] F.C. Nart, W. Vielstich, Handbook of Fuel Cells: Fundamentals, Technology, and Applications, vol. 2, John Wiley and Sons Inc., 2003, p. 302.
[26] J. Arbiol, J. Cerda, G. Dezanneau, A. Cirera, F. Peiro, A. Cornet, J.R. Morante, J. Appl. Phys. 92 (2002) 853–861.
[27] A.M. Ruiz, G. Dezanneau, J. Arbiol, A. Cornet, J.R. Morante, Chem. Mater. 16 (2004) 862–871.
[28] Y. Sato, H. Akizuki, T. Kamiyama, Y. Shigesato, Thin Solid Films 516 (2008) 5758–5762.
[29] S.J. Tauster, S.C. Fung, R.L. Garten, J. Am. Chem. Soc. 100 (1978) 170–175.
[30] S.J. Tauster, S.C. Fung, R.T.K. Baker, J.A. Horsley, Science 211 (1981) 1121–1125.
[31] S.J. Tauster, Acc. Chem. Res. 20 (1987) 389–394.